Supplementary Information

A Safe and Sustainable Bacterial Cellulose Nano-Fiber Separator for Lithium Rechargeable Batteries

Hyeokjo Gwon[1,†], Kitae Park[2,†], Soon-Chun Chung[3,†], Ryoung-Hee Kim[1], Jin Kyu Kang[2], Sang Min Ji[1], Nag-Jong Kim[3], Sunghaeng Lee[3], Jun-Hwan Ku[1], Eun Cheol Do[4], Sujin Park[3], Minsang Kim[4], Woo Yong Shim[3], Hong Soon Rhee[3], Jae-Young Kim[3], Jieun Kim[3], Tae Yong Kim[3], Yoshitaka Yamaguchi[5], Ryo Iwamuro[5], Shunsuke Saito[5], Gahee Kim[4], In-Sun Jung[4], Hyokeun Park[4], Chanhee Lee[4], Seungyeon Lee[4], Woo Sung Jeon[4], Woo Dae Jang[6], Hyun Uk Kim[6], Sang Yup Lee[6], Dongmin Im[1], Seok-Gwang Doo[4], Sang Yoon Lee[4], Hyun Chul Lee[2,*] & Jin Hwan Park[3,*]

www.pnas.org/cgi/doi/10.1073/pnas.1905527116

a

Properties of separator	BCNF	PP/PE/PP**	CCS***
Thickness (μm)	12	20	18
Porosity (%)	77	39	n.d.
Tensile strength (MPa) (MD/TD*)	63.5 / 49.9	182.3 / 13.1	83.5 / 94.4
Elongation (%) (MD/TD)	7 / 6	84 / 1220	268 / 220
Air permeability (sec per 100 cm^3)	199	547	206
Pin-puncture strength (N)	0.76	3.86	4.63
Impedance (Ω)	0.2	1.4	1.3

*MD (machine direction), TD (transverse direction), **Celgard2320, ***CK1819, Toray

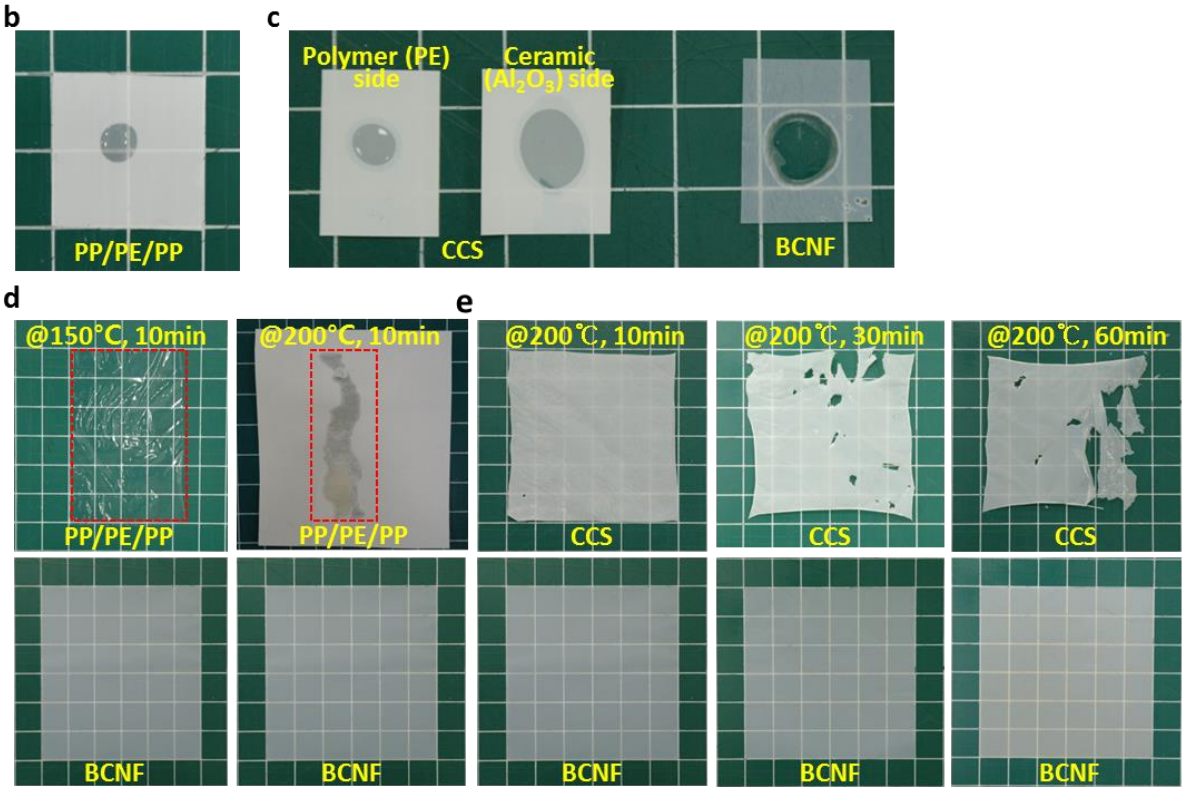

Fig. S1. Properties of the bacterial cellulose nanofiber (BCNF). (**A**) Physicochemical properties of BCNF, polypropylene/polyethylene/polypropylene (PP/PE/PP, polyolefin), and ceramic-coated separator (CCS). (**B**) Wettability of PP/PE/PP. (**C**) Wettability of CCS (polymer side (PE, left), ceramic side (Al_2O_3, right), and BCNF. (**D**) Thermal shrinkage of the PP/PE/PP (red line shows the shrunk PP/PE/PP) compared with that of BCNF. (**E**) Thermal shrinkage of

and CCS (e) compared with that of BCNF. The BCNF possesses low thermal shrinkage of less than 1% at 200 ℃

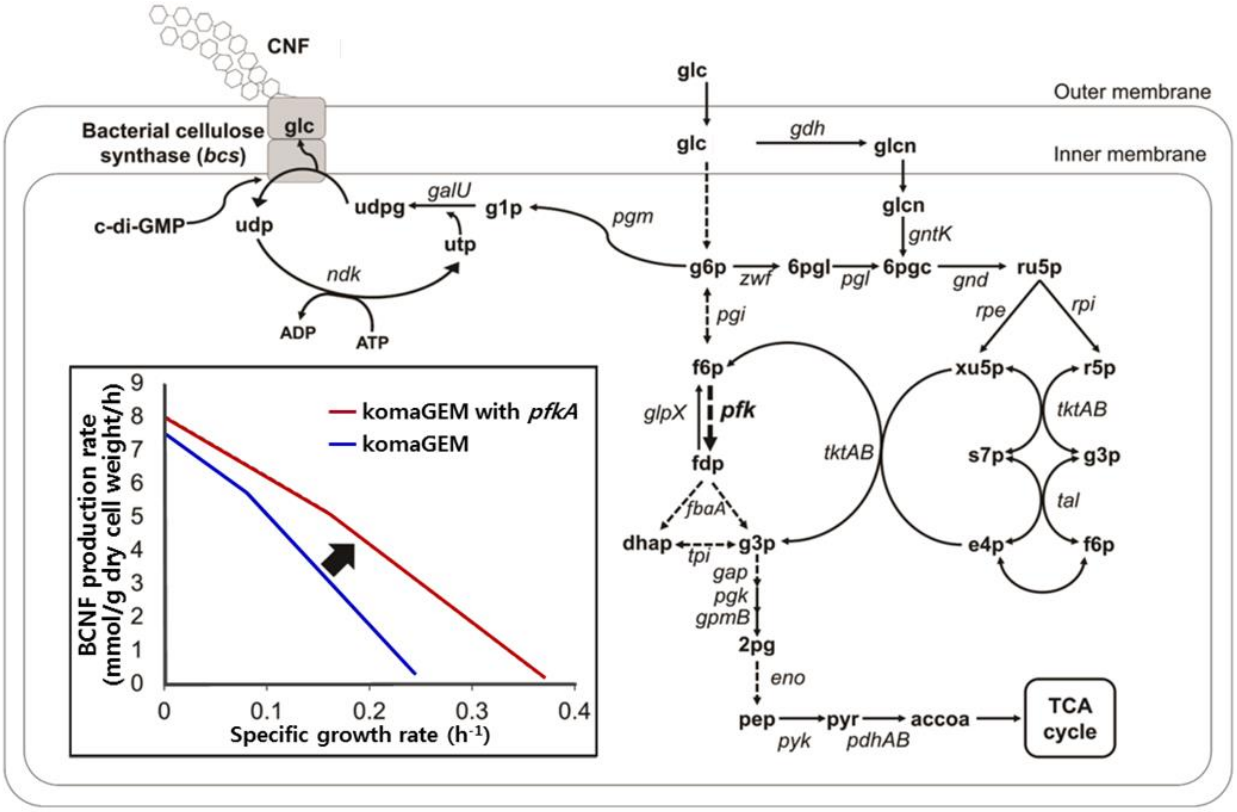

Fig. S2. Genome scale metabolic model (GEM) of *Komagataeibacter xylinus* DSM 2325 (Koma) and the simulated effect of *pfkA* gene expression on the CNF production. A GEM of Koma was reconstructed using the genome annotation data (i.e. GenBank files) of this bacterium. The complete GEM of Koma, named as komaGEM, contains information on 688 genes, corresponding to 1,712 metabolites and 1,810 reactions. Apart from transporter reactions, reactions involved in 'Amino acid metabolism' (11.1% of the total number of reactions), 'Glycan metabolism' (10.9%), 'Metabolism of cofactors and vitamins' (10.3%), and 'Carbohydrate metabolism' (8.8%) contributed to more than 40% of the reactions in the GEM. The kxyGEM was used to predict the effects of the *pfkA* gene expression on the CNF production and cell growth (inset).

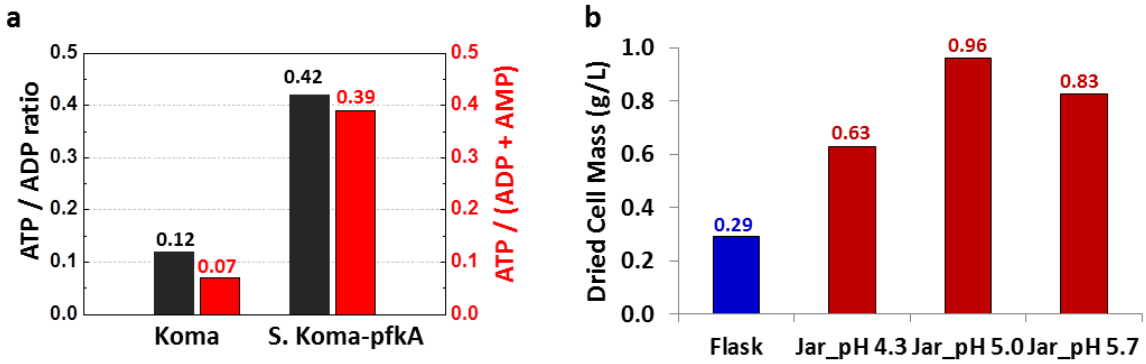

c

Strains	Glucose consumption rate (g/L/h)	Cellulose nanofiber (BCNF)			Gluconic acid (GA)	
		Production (g/L)	Productivity (g/L/h)	Yield for glucose (g/g_glucose)*100	Production (g/L)	Yield for glucose (g/g_glucose)*100
Wild type Koma (*K. xylinus* DSM2325)	1.61	3.5	0.16	9.5	22.9	64.8
S.Koma-pfkA	0.99	4.3	0.20	19.3	14.3	65.0
S.Koma-pfkA/crp	0.88	4.5	0.25	28.4	7.6	39.2
S.Koma-pfkA/crp (opt)	0.92	5.6	0.29	31.5	7.5	35.2

Fig. S3. Production of cellulose nanofibers. (**A**) Intracellular adenosine triphosphate (ATP)/adenosine diphosphate (ADP) ratio and ATP/(ADP + adenosine monophosphate (AMP)) ratio in Koma and S. Koma-pfkA strains. S. Koma-pfkA showed much higher ATP/ADP ratio (3.5 times) and ATP/(ADP+AMP) ratio (5.6 times) than those in Koma strain. (**B**) Effect of pH on the cell mass in the high seed cell process. (**C**) Cellulose nanofiber production from the Koma and optimised S.Koma-pfkA/crp (opt) strains in batch fermentation. The S.Koma-pfkA/crp strain with optimised fermentation exhibited increased BCNF production (from 3.5 to 5.6 g/L), productivity (from 0.16 to 0.29 g/L/h), and the highest yield reported so far (31.5%) with a sharply decreased yield (from 64.8 to 35.2%) of by-product, gluconic acid (GA) compared with those in wild type Koma strain.

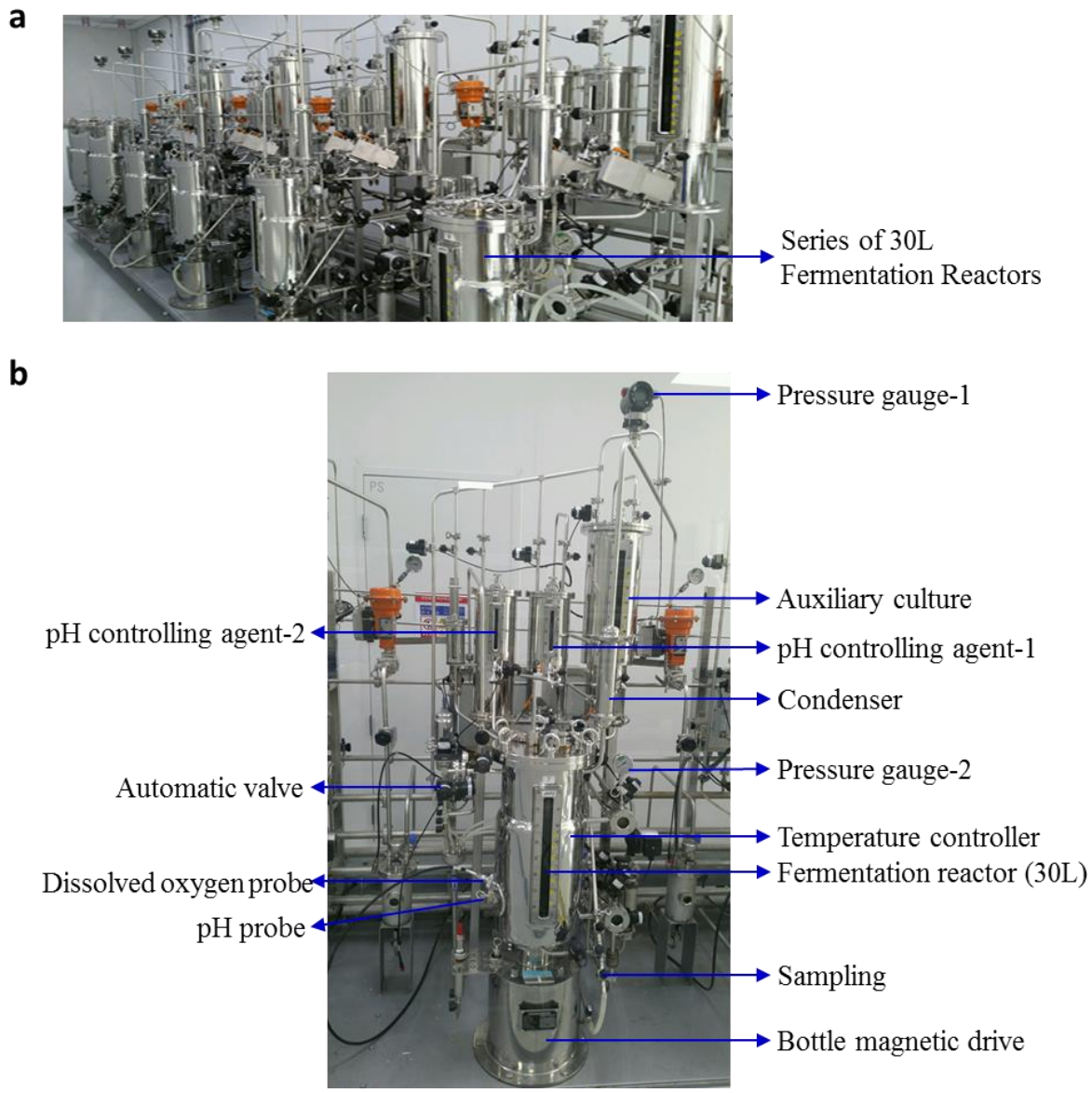

Fig. S4. Scale-up of fermentation. Mass-production of BCNF in a series of 30-L fermentation reactors. The pressure, temperature, pH, and dissolved oxygen (DO) are monitored during the fermentation.

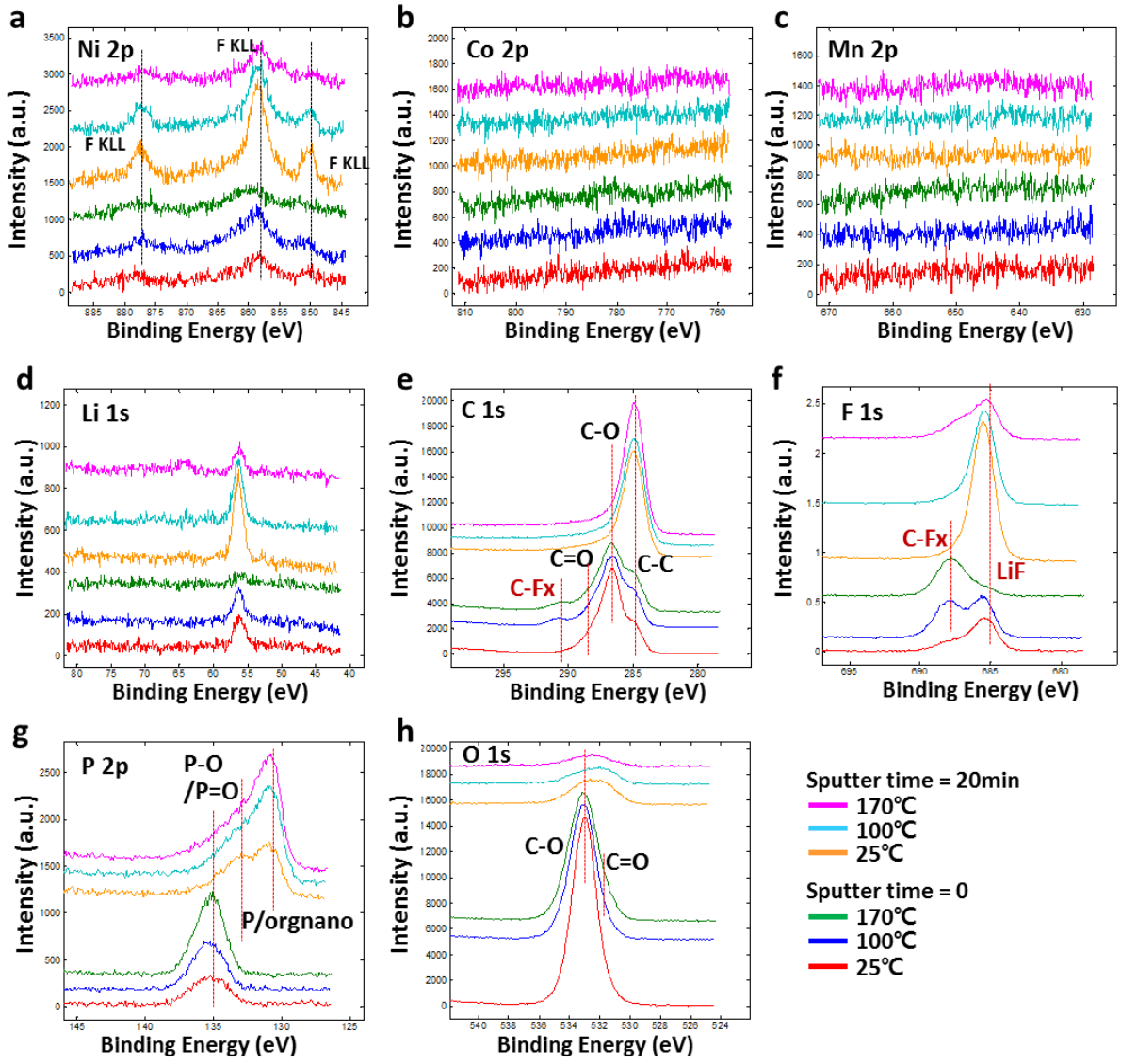

Fig. S5. X-ray photoelectron spectroscopy spectra of BCNF after heat-exposure at 170 ℃. (**A**) Ni 2p spectra. (**B**) Co 2p spectra. (**C**) Mn 2p spectra. (**D**) Li 1s spectra. (**E**) C 1s spectra. (**F**) F 1s spectra. (**G**) P 2p spectra. (**H**) O 1s spectra. The BCNF separator was obtained from the Li ion battery (LIB) full cell, which was exposed to 170 ℃, and then analysed with different sputtering times (0 and 20 min).

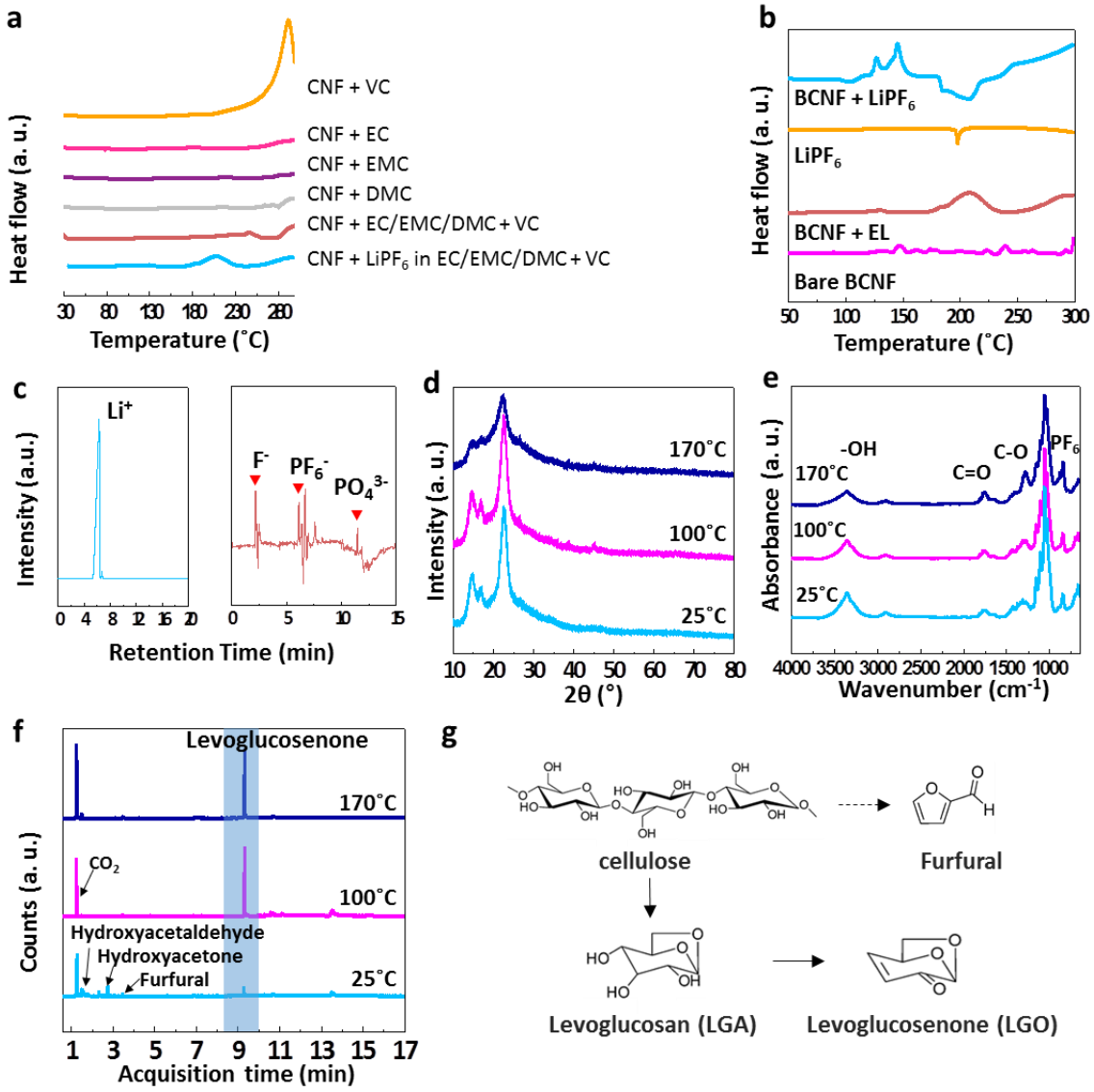

Fig. S6. Thermal safety performances and characterization of BCNF. (**A**) Differential scanning calorimetry thermograms of BCNF with each component of the electrolyte (ethylene carbonate (EC), ethyl methyl carbonate (EMC), dimethyl carbonate (DMC), vinylene carbonate (VC), and lithium hexafluorophosphate ($LiPF_6$)). An exothermic reaction occurred below 200 ℃, only when $LiPF_6$ was used. (**B**) Differential scanning calorimetry (DSC) thermograms of BCNF and its reactivity with lithium hexafluorophosphate ($LiPF_6$) and the electrolyte (EL) including

$LiPF_6$. Exothermic peaks appear only in the presence of $LiPF_6$, while no exothermic peaks in pure BCNF or $LiPF_6$. (**C**) Ionic species determined via ion chromatography of the carbonised BCNF at 170 ℃. (**D**) X-ray diffraction patterns of the BCNF. The crystallinity of BCNF decreased from 83 to 21% as the heat-exposure temperature increased from 25 to 170 ℃ in ex-situ hot-box tests. (**E**) Fourier-transform infrared (FT-IR) spectra. The intensity of the –OH bond of the BCNF decreased and those of both of the C–O bonds caused by the decomposition of the cellulose structure and PF_6 peak from $LiPF_6$, increased as the heat-exposure temperature increased from 25 to 170 ℃. (**F**) Pyrolysis-gas chromatography-mass spectroscopic analysis at 350 ℃ of BCNF after *ex-situ* heat-exposure in the presence of the electrolyte including $LiPF_6$ at 25, 100, and 170 ℃, respectively. (**G**) Possible pathways for the transformation of BCNF to the pyrolysed products.

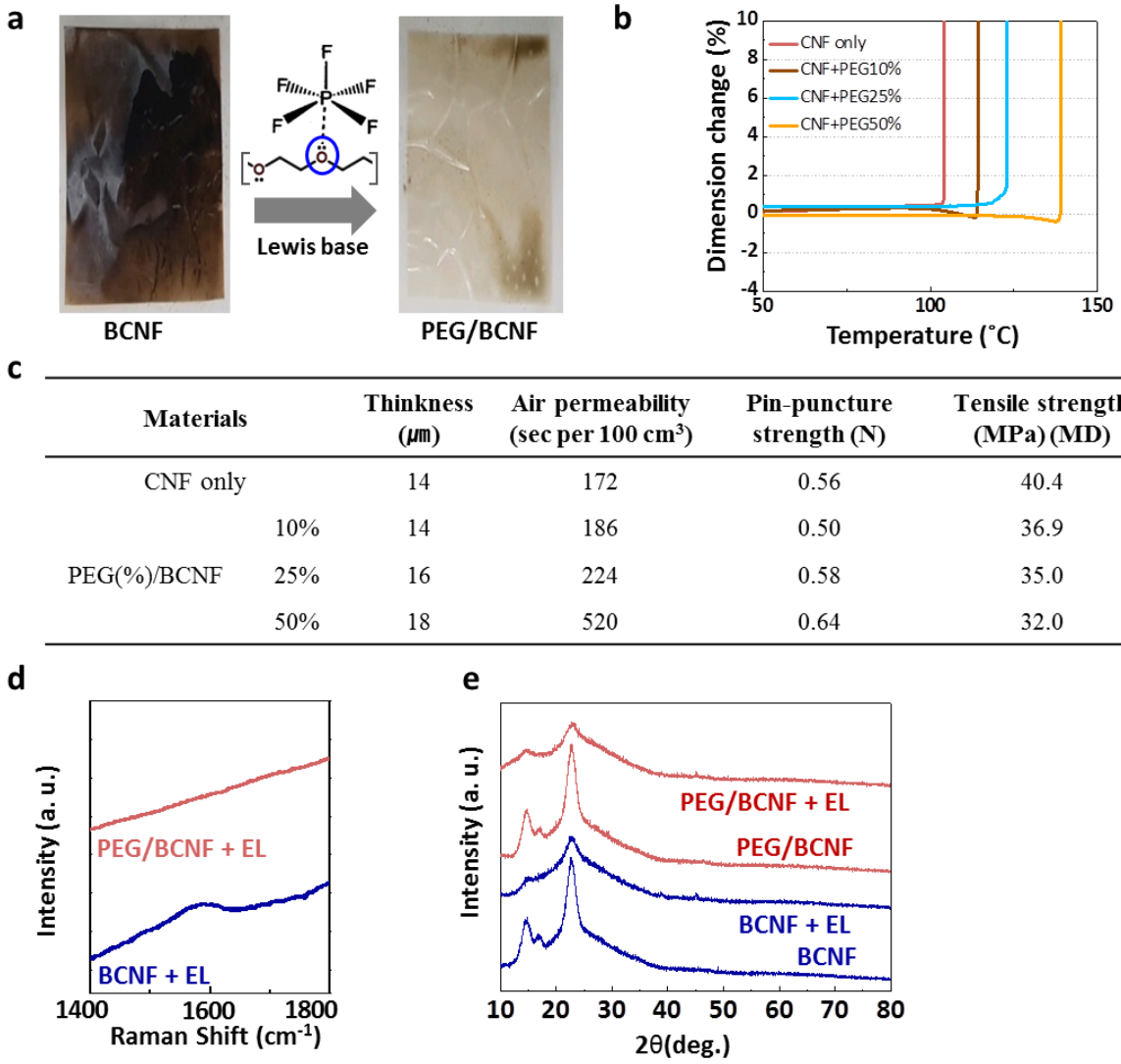

c

Materials		Thinkness (μm)	Air permeability (sec per 100 cm^3)	Pin-puncture strength (N)	Tensile strength (MPa) (MD)
CNF only		14	172	0.56	40.4
PEG(%)/BCNF	10%	14	186	0.50	36.9
	25%	16	224	0.58	35.0
	50%	18	520	0.64	32.0

Fig. S7. Characterization of PEG/BCNF. (**A**) Photographs of a BCNF membrane in a battery with $LiPF_6$ in comparison with that in an electrolyte containing polyethylene glycol (PEG) as well. It was observed that the carbonisation of BCNF was alleviated, when PEG was added to the electrolyte (25%). (**B**) TMA analysis of the BCNF and PEG/BCNFs mixed with an electrolyte. The PEG was directly added into the BCNF during membrane manufacture process. When mixed with the electrolyte, BCNF exhibited a sharp decrease in thermal resistance to 104 ℃, compared to BCNF only (338 ℃ in Fig. 3D). The thermal resistance improved up to 140 ℃ as

the amount of PEG added was increased (up to 50%). (**C**) Properties of the PEG/BCNF with different amounts of PEG (10, 25, and 50%). The PEG(25%)/BCNF membrane exhibited reasonable properties such as tensile strength of ~35 MPa, air-permeability of 224 s/100 cm^{-3}, and applied as a separator in LIB. (**D**) Raman spectra of BCNF and PEG/BCNF. The C–C bond on the carbonised BCNF decreased on the PEG/BCNF. (**E**) X-ray diffraction patterns of BCNF and PEG(25%)/BCNF. After heat-treating at 170 ℃ in the presence of an electrolyte including $LiPF_6$, the decrease in the crystallinity (67 to 46%) of the PEG(25%)/BCNF membrane was much more mitigated than that of the BCNF membrane (83 to 21%).

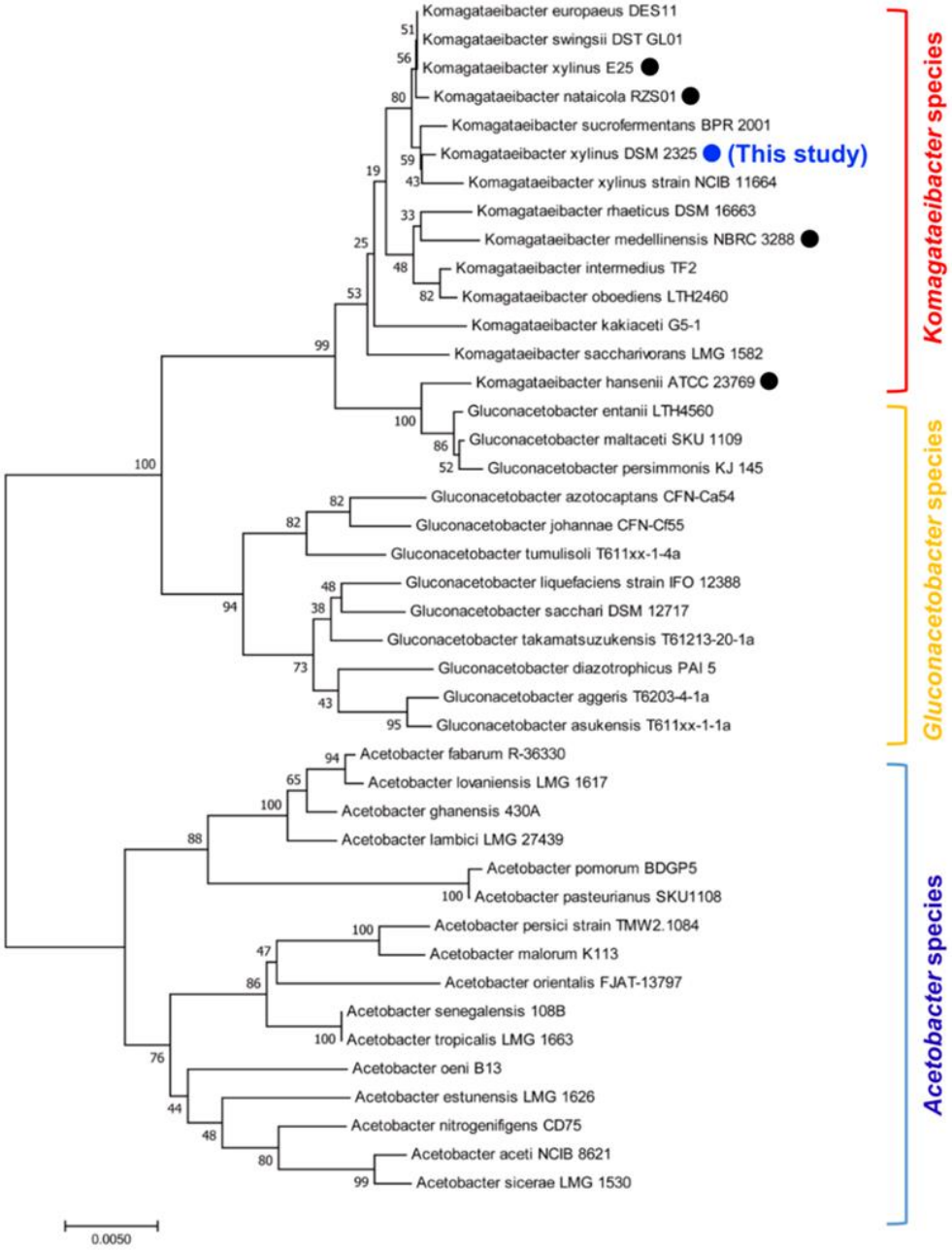

Fig. S8. Phylogenetic relationship of bacteria belonging to the Acetobacteraceae family based on their 16S rRNA sequences. Genome of *Komagataeibacter xylinus* DSM 2325 was newly sequenced in this study (blue dot). The four *Komagataeibacter* species with black dots have complete genome sequences. The 16S rRNA gene based-phylogenetic tree was constructed using the neighbour-joining method[1] of MEGA 7.0[2]. The sequences were aligned using

MUSCLE[3] within MEGA 7.0. Percentages of replicate trees for the associated taxa clustered together in the bootstrap test (1,000 replicates) are shown next to the branche[4]. Evolutionary distances were computed using the p-distance method in units of the number of base substitutions per site[5].

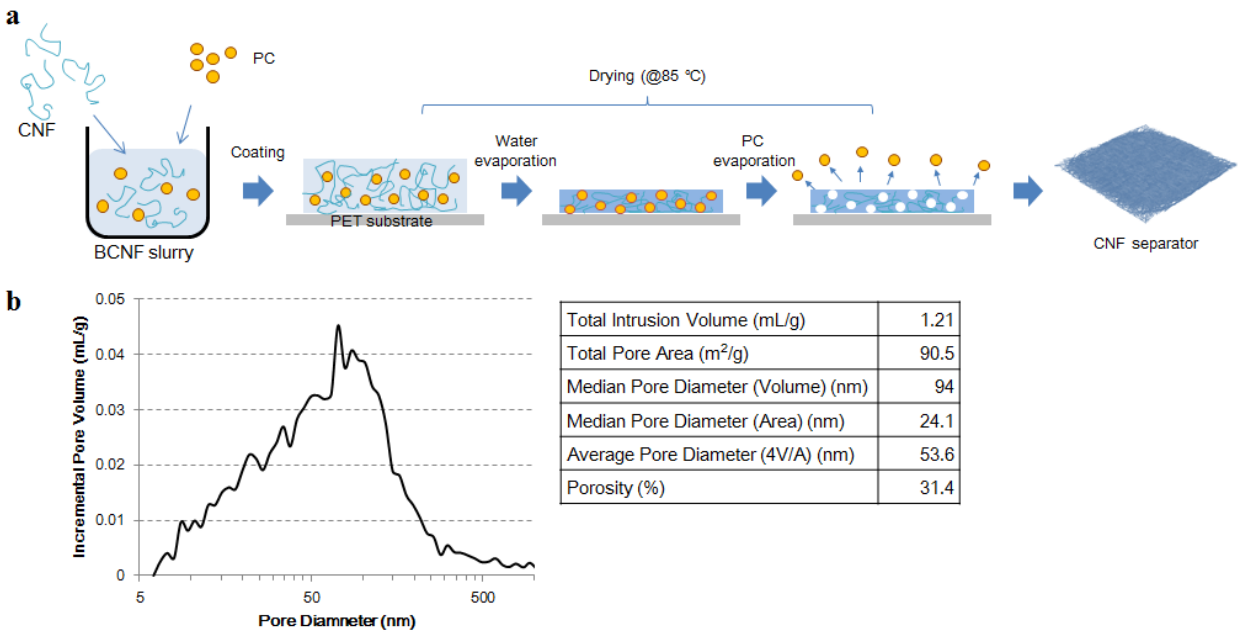

Total Intrusion Volume (mL/g)	1.21
Total Pore Area (m^2/g)	90.5
Median Pore Diameter (Volume) (nm)	94
Median Pore Diameter (Area) (nm)	24.1
Average Pore Diameter (4V/A) (nm)	53.6
Porosity (%)	31.4

Fig. S9. Preparation and characterization of BCNF non-woven separator. a, The Slurry of BCNF mixed with PC, as foam making agent, was coated on PET substrate. During drying, as water evaporates first, the matrix of BCNF was constructed and then PC, which has lower volatility, evaporates to form pores. Fully dried BCNF film is easily detached from substrate. **b,** The pore size distribution and porosimetric values of BCNF separator from mercury porosimeter analysis (Autopore IV9500, Micromeritics).

1 Table S1. Koma strains and plasmids constructed and used in this study

Strains and plasmids	Genotype & Descriptions	Reference
Strains		
Koma (K. xylinus DSM 2325)	Wild-type strain	DSMZ
S.Koma-Δ2760	DSM 2325, Δ2760	This work
S.Koma-pfkA	DSM 2325, Δ2760_P_{tac}::pfkA (from E. coli MG1655)	This work
S.Koma-Δ0648	S. Koma-pfkA, Δ0648	This work
S.Koma-pfkA/crp	S. Koma-pfkA, Δ0648_P_{tac}::crp	This work
Plasmids		
pMSK+	Vector for cloning; Kan^R	This work
pTSK+	Vector for allelic exchange in *K. xylinus*; tetA	This work
pTSa	Shuttle vector for *K. xylinus*; tetA	This work
pTSa-EX1	Vector for overexpression under the control of tac promoter; tetA	This work
pTSa-EX2	Vector for overexpression under the control of gapA promoter; tetA	This work
pTSa-pfkA	Cloning pfkA gene into BamHI site of pTSa-EX1; tetA	This work
pTSa-pgi	Cloning pgi gene into BamHI site of pTSa-EX1; tetA	This work
pTSa-pgk	Cloning pgk gene into BamHI site of pTSa-EX1; tetA	This work
pTSa-fba	Cloning fba gene into BamHI site of pTSa-EX1; tetA	This work
pTSa-tpi	Cloning tpi gene into BamHI site of pTSa-EX1; tetA	This work
pTSa-gap	Cloning gap gene into BamHI site of pTSa-EX1; tetA	This work
pTSa-gpm	Cloning gpm gene into BamHI site of pTSa-EX1; tetA	This work
pTSa-pck	Cloning pck gene into BamHI site of pTSa-EX1; tetA	This work
pTSa-mae	Cloning mae gene into BamHI site of pTSa-EX1; tetA	This work
pTSK-Δ2760	Vector for deletion of Gene_2760 of the K. xylinus DSM 2325	This work
pTSK-Δ2760-Ec.pfkA	Vector for integration of E. coli pfkA gene; tetA	This work
pIN01	Vector for deletion of Gene_0648 of the K. xylinus DSM 2325; cm^R	This work
pIN01-crp	Vector for integration of crp (Gene_2117) under the control of gapA promoter; cm^R	This work

1 Table S2. Primers used for gene cloning and deletion

Primer	Sequence
MD-058	5’-TATTGAAAAAGGAAGAGTATGATTGAACAAGATGGATTGCACGCAGGT-3’
MD-059	5’-AGTAAACTTGGTCTGACATCAGAAGAACTCGTCAAGAAGGCGATAGAA-3’
MD-060	5’-ACTCTTCCTTTTTCAATATTATTGAAGCA-3’
MD-061	5’-TGTCAGACCAAGTTTACTCATAT-3’
P1646	5’-CTTGATATCGAATTCTTCTCATGTTTGACAGCTTATCATC-3’
P1647	5’-GGGCTGCAGGAATTCGAATTTCTGCCATTCATCCGC-3’
P1662	5'-CTTGATATCGAATTAGGCCTGTCATCGTCTATATACG-3'
P1663	5'-CGTGTTGTTCGAATTCGATGGATATTCCTCCAGTATCATGTG-3'
P1664	5'-CATCGAATTCGAACAACACGCCGATGTATGAC-3'
P1665	5'-ACATGAGAAGAATTGACAGATCCGGTCAGTTCACATTATC-3'
Ec.pfkA_F	5’-CGTACCCGGGGATCCATGATTAAGAAAATCGGTGTGTTG-3’
Ec.pfkA_R	5’-GACTCTAGAGGATCCTTAATACAGTTTTTTCGCGCAGTC-3’
pgi_F	5'-TCCTCTAGAGTCGACATGAGTGCGCGTGAATCTG -3'
pgi_R	5'-TGCCTGCAGGTCGACTCAGACCGCGTGGGCGATATC -3'
pgk_F	5'-TCCTCTAGAGTCGACATGGGTGCGGCAAGCTTC-3'
pgk_R	5'-TGCCTGCAGGTCGACTCAGATGGGCATGGCCCG-3'
fba_F	5’-TCCTCTAGAGTCGACATGCCTATTGATCAGATGCGC -3’
fba_R	5’-TGCCTGCAGGTCGACTCAGACCTTTTGCGTCGAAG -3’
tpi_F	5'-TCCTCTAGAGTCGACATGAAACAGATCATTGTTGGCAAC-3'
tpi_F	5'-TGCCTGCAGGTCGACTCACGATGCGCGGGCGG-3'
gapA_F	5'-TCCTCTAGAGTCGACATGGCTGTTAAAGTCGCAATAAAC-3'
gapA_R	5'-TGCCTGCAGGTCGACTTACAGGGCACCGAATACG-3'
pgk_F	5’-TCCTCTAGAGTCGACATGGGTGCGGCAAGCTTC-3’
pgk_R	5’-TGCCTGCAGGTCGACTCAGATGGGCATGGCCCG-3’
gpm_F	5’-TCCTCTAGAGTCGACATGAACGACCATGAATCGATGAAC-3’
gpm_R	5’-TGCCTGCAGGTCGACTCAGGATGGCGTGGACC-3’
pck_F	5’-TCCTCTAGAGTCGACATGACCGAAGCCGCCGC-3’
pcK_R	5’-TGCCTGCAGGTCGACTTAGCCAAAAGCGCCAACATG-3’
mae_F	5’-TCCTCTAGAGTCGACATGTCGGACACAGTGCG-3’
mae_R	5’-TGCCTGCAGGTCGACTCAGGCTTTTTCGTACGGG-3’
P1678	5’-ATATCCATCGAATTCGGAGCTTATCGACTGCACG-3’
P1679	5’-GTGTTGTTCGAATTCAAAAGGCCATCCGTCAGG-3’
0648up_infF	5’-GACGGCCAGTGAATTTGGCACCATACATTCCGGTTTCCC-3’
0648up_infR	5’-CGACCTGCACAGCCAAGACCATGCCTTGCCCGTTATCG-3’
0648dn_infF	5’-TGGCCTTTTTGCCTTAGGCATCCGTTCGCACGATACCTG-3’
0648dn_infR	5’-ATGATTACGCCAGCTTAATATGGCAGCCATCAATACCCC-3’
Ptac_F	5’-GGCTGTGCAGGTCGTAAATCACTGC-3’
Ptac_R	5’-TTTCTCCATCAATAGCTCGTCCCTCCTTCTTTCTAGAGAGCTCGGTACCCGGGAGATCTATGTTTCCTGTGTGAAATTG-3’
Cat-F	5’-CGAGCTATTGATGGAGAAAAAAATCACTGG-3’
Cat-R	5’-GGGCACCAATAACTGCCTTAAAA -3’
P-mcs-infF	5’-CAGTTATTGGTGCCCAACGAATCACCTGTAAGTCGGACGC -3’
P-mcs-infR	5’-AAGGCAAAAAGGCCATCCGTCAGG -3’
2117-infF	5’-TAGAGTCGACCTGCATGAAAGTGAATTGGAAATTATC-3’
2117-infR	5’-GCTTGCATGCCTGCACTAGCCGTTGCCTGCGGCCAG -3’
pUC19-F	5’-ACACGGTGCCTGACTGCGTTAGCAATTTAACTGTG -3’
pUC19-R	5’-ATGGAAGCCGGCGGCACCTCGCTAACGGATTCACCACTCCAAG -3’
Tet-F	5’-CGCAGTCAGGCACCGTGTATGAAATCTAACAATGCGCTCATCGTCATCCTC-3’
Tet-R	5’-GGTGCCGCCGGCTTCCATTCAGGTCGAGGTGGCCCGGCTCCATG-3’
pSa-F	5’-GCCAGCAAGACAGCGATAGAGGGTAGTTATCCACGTGAAAC -3’
pSa-R	5’-CGACTTACAGGTGATCGGAAATCCAGAAGCCCGAGAGGTTG -3’
EX1_infF	5’-CTGACGGATGGCCTTTTTGCCTTCCGCTTCCTCGCTCACTGACTC-3’
EX1_infR	5’-TCTACGCCGGACGCATCGCGTCCGACTTACAGGTGATCGGAAAT-3’
Ptac_infF	5’-CGATGCGTCCGGCGTAGAGGATCCGGAGCTTATCGACTG -3’
Ptac_infR	5’-CGAGCTCGGTACCCAATCAATAGCTCGTCCCTGTGTGAAATTGTTATCCGCTCAC-3’
EX1-MCS_infF	5’-ATTGGGTACCGAGCTCGAATTCGTACCCGGGGATCCTCTAGAGTCGAC -3’
TrrnB_infR	5’-GCAAAAAGGCCATCCGTCAGGATGGCC -3’
EX2_infR	5’-CGGGCGCCGCCGAAGTTGCGTCCGACTTACAGGTGATCGGAAAT-3’
PgapA_infF	5’-AACTTCGGCGGCGCCCGAGCGTGAACAGCAC-3’
PgapA_infR	5’-CGAGCTCGGTACCCAATTTTCTTATTTTCTCCGTAAGGTCTGAC-3’

Table S3. Number of genes from *Komagataeibacter xylinus* DSM 2325 for each clusters of orthologous groups (COG) functional category using eggNOG-mapper[6, 7]

COG functional category	Number of genes	% of total	Description
A	0	0.00	RNA processing and modification
B	0	0.00	Chromatin structure and dynamics
C	168	6.65	Energy production and conversion
D	22	0.87	Cell cycle control, cell division, chromosome partitioning
E	218	8.62	Amino acid transport and metabolism
F	77	3.05	Nucleotide transport and metabolism
G	135	5.34	Carbohydrate transport and metabolism
H	110	4.35	Coenzyme transport and metabolism
I	59	2.33	Lipid transport and metabolism
J	150	5.93	Translation, ribosomal structure and biogenesis
K	140	5.54	Transcription
L	282	11.16	Replication, recombination and repair
M	174	6.88	Cell wall/membrane/envelope biogenesis
N	4	0.16	Cell motility
O	106	4.19	Posttranslational modification, protein turnover, chaperones
P	175	6.92	Inorganic ion transport and metabolism
Q	34	1.34	Secondary metabolites biosynthesis, transport and catabolism
R	0	0.00	General function prediction only
S	513	20.29	Function unknown
T	76	3.01	Signal transduction mechanisms
U	47	1.86	Intracellular trafficking, secretion, and vesicular transport
V	38	1.50	Defence mechanisms
W	0	0.00	Extracellular structures
Y	0	0.00	Nuclear structure
Z	0	0.00	Cytoskeleton
	2,528		

Table S4. Genes associated with the bacterial cellulose biosynthesis

locus_tag ID	KEGG orthology (KO)	[c] Definition
Bacterial cellulose synthesis		
[a]GENE_02676 [a]GENE_02677 [a]GENE_00599 GENE_01096 [a]GENE_02507 [a]GENE_02510	K00694 K20541	Cellulose synthase (UDP-forming) (BcsA) Cellulose synthase operon protein B (BcsB)
[a]GENE_02678 [a]GENE_00602 [a]GENE_02511	K20543	Cellulose synthase operon protein C (BcsC)
[a]GENE_02679	No KO assigned	Cellulose synthase operon protein D (BcsD)
[a]GENE_00600	No KO assigned	BcsX
[a]GENE_00601	No KO assigned	Putative membrane-bound transacylase (BcsY)
Regulation of the bacterial cellulose synthesis		
[a]GENE_02674 GENE_02984	K01179	Endoglucanase
[a]GENE_02680 GENE_02541	K01188	Beta-glucosidase
[b]GENE_02262 [b]GENE_00259 [b]GENE_00422 [b]GENE_01580 [b]GENE_01742 GENE_00123 GENE_00656 GENE_00991 GENE_01825	K13069	Diguanylate cyclase
[b]GENE_02263 [b]GENE_00260 [b]GENE_00421 [b]GENE_01578 [b]GENE_01579 [b]GENE_01743	K07181	Phosphodiesterase

[a] Genes found in *bcs* operons

[b] Genes found in *cdg* operons

[c] Enzyme names retrieved from KEGG database

Table **S5. Number of core genes from the five *Komagataeibacter* species for each COG functional category using eggNOG-mapper[6, 7]**

COG functional category	Number of genes	% of total	Description
A	0	0.00	RNA processing and modification
B	0	0.00	Chromatin structure and dynamics
C	118	7.33	Energy production and conversion
D	18	1.12	Cell cycle control, cell division, chromosome partitioning
E	143	8.88	Amino acid transport and metabolism
F	61	3.79	Nucleotide transport and metabolism
G	85	5.28	Carbohydrate transport and metabolism
H	102	6.34	Coenzyme transport and metabolism
I	40	2.48	Lipid transport and metabolism
J	135	8.39	Translation, ribosomal structure and biogenesis
K	76	4.72	Transcription
L	89	5.53	Replication, recombination and repair
M	119	7.39	Cell wall/membrane/envelope biogenesis
N	2	0.12	Cell motility
O	90	5.59	Posttranslational modification, protein turnover, chaperones
P	98	6.09	Inorganic ion transport and metabolism
Q	20	1.24	Secondary metabolites biosynthesis, transport and catabolism
R	0	0.00	General function prediction only
S	313	19.44	Function unknown
T	49	3.04	Signal transduction mechanisms
U	30	1.86	Intracellular trafficking, secretion, and vesicular transport
V	22	1.37	Defence mechanisms
W	0	0.00	Extracellular structures
Y	0	0.00	Nuclear structure
Z	0	0.00	Cytoskeleton
	1,610		

Table S6. Maximal titers, yields, and productivity levels of BCNF-producing strains as described previously.

Strains	C-source	CNF Production (g/L)	Yield per reduced sugar (wt%)	Fermentation Time (hr)	Fermentation Type	Reference
S.Koma-pfkA/crp	Glucose	5.6	31.5	19.5	30L Batch Fermentor	In this study
Acetobacter xylinum BPR2001	Fructose	8	20	67	50L Internal-Loop Airlift Reactor	8
Acetobacter xylinum BRC 5	Glucose	15.3	26	50	5L Fed batch Fermentor	9.
Acetobacter xylinum ssp. *sucrofermentans* BPR2001	Fructose	10.4	11.6	52	50L internal-loop airlift reactor	10
Gluconacetobacter xylinus ATCC 23770	Fiber sludges	10-11	30	168	Static culture	11

Methods

Bacterial strains, culture media, and conditions

The Koma strains and plasmids used and constructed in this study are listed in table S1. The wild-type *Komagataeibacter xylinus* DSM 2325 (Koma) strains were obtained from the Leibniz Institute DSMZ (German Collection of Microorganisms and Cell Cultures) (Braunschweig, Germany). The Koma strains were usually grown in the Hestrin-Schramm (HS) medium (0.5% yeast extract, 0.5% peptone, 0.375% Na_2HPO_4, 0.115% citric acid, pH 4.5) supplemented with 2% glucose, and then cultured at 30 °C. For the production of cellulose nanofibers, 1% (v/v) ethanol was added to the HS medium.

Construction of plasmids

The oligonucleotides used in this study are listed in table S2. For the construction of pMSK+, the kan^R gene from pK19-mobsacB and vector backbone from pBluescript II SK (+) (Stratagene) were amplified using two pairs of oligonucleotides designated as MD-058 / MD-059 and MD-060 / MC-061, respectively. After purification, the PCR fragments were cloned using In-Fusion® HD Cloning Kit (Clonetech). For the construction of pTSK+, the tetA gene from pBR322 (ATCC) was amplified using the P1646/P1647 primer set. The obtained PCR fragment was purified and cloned into EcoRI restriction site of the pMSK+ vector using the In-Fusion® HD Cloning Kit. For the construction of pTSa shuttle vector, the pUC origin from puc19 and tetA resistance gene from pBR322 (ATCC) DNA fragments were amplified using two pairs of oligonucleotides designated as pUC19-F/R and tet-F/R, respectively. After purification, the PCR fragments were cloned using the In-Fusion® HD Cloning Kit, which resulted in pUC-tet. pSa originating from pUCD2 (ATCC) was amplified using pSa-F/R primers. After purification, the

PCR fragments were cloned into the EcoRI restriction site of pUC-tet the using In-Fusion® HD Cloning Kit. The pTSa-EX1 and pTSa-EX2 were constructed for the overexpression of genes under the control of tac or gapA promoter. To construct the pTSa-EX1 vector, the vector region of pTSa and Ptuf::MCS::TrrnB DNA fragments from the pTac15K vector were amplified using EX1_infF/R, Ptac_infF/R, and EX1-MCS_infF/TrrnB_infR primer sets, respectively. After purification, the PCR fragments were cloned using the In-Fusion® HD Cloning Kit. For the construction of the pTSa-EX2 vector, the vector region of pTSa-EX1 and gapA promoter from *K. xylinus* DSM 2325 were amplified using two pairs of oligonucleotide designated as EX1-MCS_infF/EX2_infR and PgapA_infF/R, respectively. After purification, the PCR fragments were cloned using the In-Fusion® HD Cloning Kit. For the overexpression of *pfkA from E. coli MG1655, pgi*, *pgk*, *fba*, *tpi*, *gap*, *pgk*, *gpm*, *pck,* and *mae* genes from *K. xylinus* DSM 2325, ORFs were amplified using oligonucleotide pairs and cloned into BamHI or SalI restriction site of the pTSa-EX1 vector using the In-Fusion® HD Cloning Kit. For the construction of pTSK-*Δ2760*, the region up- and down-stream of the Gene_2760 were amplified using two pairs of oligonucleotides designated as P1662/P1663 and P1664/P1665, respectively. After purification, the PCR fragments were cloned into EcoRI restriction site of pTSK+ using In-Fusion® HD Cloning Kit. The pTSK-*Δ2760*_Ec.pfkA was constructed for the integration of the *E. coli pfkA* gene. The tac promoter, pfkA gene, and rrnB terminator were amplified from pTSa-Ec.pfkA using the P1678 and P1679 primer sets. After purification, the PCR fragments were cloned into EcoRI restriction site of pTSK-*Δ2760* using the In-Fusion® HD Cloning Kit. The pIN01 was constructed for the deletion of the Gene_0648 gene. The region up- and down-stream of the Gene_0648 were amplified using two pairs of oligonucleotides designated as 0648up_infF/R and 0468dn_infF/R, respectively. The tac promoter from pTSa-EX1, chloramphenicol resistance

gene from pBR322, and PgapA-MCS-TrrnB cassette from pTSa-EX2 were amplified using Ptac_F/R, cat_F/R, and P-mcs-infF/R primer sets, respectively. After purification, the PCR fragments were cloned into EcoRI and HindIII restriction site of pUC19 using the In-Fusion® HD Cloning Kit. For the construction of pIN01-crp, the crp gene (Gene_2117) from *K. xylinus* DSM 2325 was amplified using the 2117_infF/R primer set. After purification, the PCR fragments were cloned into PstI restriction site of pIN01 using the In-Fusion® HD Cloning Kit.

Abbreviations of gene and metabolites

Genes

gdh: glucose dehydrogenase; zwf: glucose 6-phosphate 1-dehydrogenase; pgl: 6-phosphogluconolactonase; gnd: 6-phosphogluconate dehydrogenase; rpe: ribulose-phosphate 3-epimerase; rpi: 6-phosphogluconate dehydrogenase; tkt: transketolase; tal: transaldolase; pgi: glucose-6-phosphate isomerase; pfkA: 6-phosphofructokinase A; fbaA: fructose bisphosphate aldolase A; tpi: triosephosphate isomerase; gap: glyceraldehyde 3-phosphate dehydrogenase; pgk: phosphoglycerate kinase; gpmB: 2,3-bisphosphoglycerate-independent phosphoglycerate mutase B; eno: enolase; pyk: pyruvate kinase; pdhAB: pyruvate dehydrogenase AB; pgm: phosphoglucomutase; ugp: UTP-glucose-1-phosphate uridylyltransferase; ndk: nucleoside-diphosphate kinase.

Metabolites

glc: glucose; glcn: gluconate; g6p: glucose 6-phosphate; 6pgl: 6-phosphogluconolacton; 6pgc: 6-phosphogluconate; ru5p: ribulose-5-phosphate; r5p: ribose-5-phosphate; xu5p: xylulose-5-phosphate; s7p: sedoheptulose; e4p: erythrose 4-phosphate; g3p: glyceraldehyde-3-phosphate; f6p: fructose 6-phosphate; f16p: fructose-1,6-diphosphate; dhap: dihydroxyacetone phosphate;

2pg: 2-phosphoglyceric acid; pep: phosphoenol pyruvate; pyr: pyruvate; g1p: glucose 1-phosphate; udpg: UDP-glucose; c-di-GMP: cyclic diguanylate.

Genome sequencing of Komagataeibacter xylinus DSM 2325

Genome sequencing of Koma revealed that this bacterium has the genome of 3,727,795 base pairs (bp), consisting of a circular chromosome (3,353,346 bp) and two plasmids (369,140 and 5,309 bp), with an average guanine (G) + cytosine (C) content of 58.9%. Comparative genome analysis was performed on Koma and other five *Komagataeibacter* species (table S3 to S5). A result of the classification of genes according to the clusters of orthologous groups (COG) functional categories revealed that 'Replication, recombination, and repair' (11.2%) and 'Amino acid transport and metabolism' (8.6%) were the two subsystems associated with the greatest number of genes with the exception of 'Function unknown' (20.3%) (table S3). Genes associated with the CNF biosynthesis were also found in the genome of Koma, including *glk* encoding glucokinase, *pgm* encoding phosphoglucomutase, *galU* encoding UTP-glucose-1-phosphate uridylyltransferase, and *bcs* operon (*bcs*ABCD genes) (table S4).Genome analysis also confirmed that the wild-type Koma does not have the phosphofructokinase (*pfkA*) gene in glycolysis, but has a full set of genes for pentose phosphate pathway (PPP). The genome was sequenced using Illumina HiSeq 2500 (Illumina, San Diego, CA) and PacBio RS II system (Pacific Biosciences, Menlo Park, CA). Illumina and PacBio reads were assembled using SPAdes[12] and HGAP[13], respectively. The assembled contigs from the two sequencing approaches were merged using GARM[14]. Among a total of 48,560,562 Illumina reads generated, 47,301,277 reads (97.41%) were mapped to the assembled genome, which validated the quality of the finished genome sequence. Genome annotation was implemented using PGAP[15].

Sequences of one chromosome and two plasmids of the wild-type Koma have been deposited in the NCBI GenBank under the accession numbers, CP025269 to CP025271 (fig. S8).

Construction of metabolically engineered strains and plasmids

The metabolically engineered Koma strains were constructed by a homologous recombination procedure, as described previously[16]. To construct S. Koma-*Δ*2760, S. Koma-pfkA, and S. Koma-pfkA/crp, 10 μL of a plasmid DNA (pTSK-Δ2760, pTSK-Δ2760-Ec.pfkA, or pIN01-crp) was added to 100 μL of competent cells. Then, the cell/DNA mixture was transferred to a cold 2-mm electroporation cuvette and a pulse was applied. Cells were transferred to 1 mL of an HS medium containing 0.2% cellulase in a 14-mL round tube and incubated overnight at 30 ℃ with shaking. Subsequently, the cells were spread on a HS agar plate supplemented with tetracycline (10 μg/mL) or chloramphenicol (200 μg/mL). The primers used for gene cloning and deletion are listed in Table S2. Detailed procedures for the construction of plasmids and the abbreviations of the genes and metabolites are provided in the Supporting Information. All DNA manipulations were carried out using standard protocols[17].

Computational fluid dynamics methodology and kLa measurement

Computational fluid dynamics (CFD) can be used to simulate and optimise mixing, shear stress, and mass transfer coefficients. CFD was performed using NX (3D CAD) and FLOW-3D (general-purpose CFD package software). The model system consisted of a 2.5-L standard stirred tank reactor filled with 1.4 L of the fermentation medium. Among the various multiphase models, the Volume of Fluid (VOF) model was chosen to model the turbulence between fermentation medium and air using the momentum and volume fraction equations. The reactor model contained grids with a total of up to 6×10^5. The impellers and reactor walls were

treated as non-slip boundaries with standard wall functions. Impeller rotation was simulated using general moving objects (GMO) model in steady state simulations. From multiphase simulations using the VOF model, the turbulent energy and shear stress were predicted for various impeller types (Rushton, Pitch-blade, modified pitch-blade), agitation speeds (50–350 rpm), and viscosity (1–40 cP). The volumetric oxygen-transfer coefficient (k_La) represents the capacity of the oxygen supply, which is related to the impeller type, reactor configuration, agitation speed, and aeration rate. The k_La was determined by a dynamic (unsteady-state) method. In this method, the reactor is first deoxygenated by sparging nitrogen gas until DO reaches below 20% saturation level. Then, the air is reintroduced into the fermenter while the DO reaches about 80% saturation value. The k_La was determined at an agitation speed of 50–350 rpm, aeration rate of 1.4 L/min, temperature of 30 °C, and viscosity of 1–40 cP.

$$dDO/dt = k_La\ (DO_{sat} - DO)$$

BCNF production by CMC-based fermentation

The high seed cell process, which is one of the most cost-effective means of achieving high CNF productivity, was performed to maximise the cell mass and activity by adjusting the culture conditions, including temperature, pH, and medium. A maximum dry cell mass of 0.96 g/L was obtained at a seed pH of 5.0 (fig. S3). The seed culture was prepared by a two-step fermentation process. In the first seed culture process, Koma strain grown in HS agar medium, was inoculated into a 250-mL Erlenmeyer flask containing 100 mL of the HS medium at 150 rpm for 10 h. The temperature was maintained at 30 °C in all the cultures, unless otherwise indicated. The second seed culture was performed in a 1.0-L jar fermenter (HANIL science; South Korea) containing 0.7 L of a medium composed of 35 g/L glucose, 1 g/L yeast extract, 2

g/L monosodium glutamate (MSG), 0.5 g/L $MgSO_4 \cdot 7H_2O$, 1.0 g/L KH_2PO_4, 1.15 g/L citric acid, 10 mM sodium acetate buffer (pH 4.7), and 10 g/L Na-CMC under 250 rpm and aeration rate of 0.7−1.0 L/min. Most of fermentation parameters were assessed in a 2.5-L jar fermenter (New Brunswick Fermentation systems Bioflo 310, USA) containing 1.4 L of the medium under 250−350 rpm and an aeration rate between 1.4 and 2.1 L/min, depending on the culture time. The pH was controlled at 5.0 using a 3 N KOH solution. The supplementation of oxygen-enriched air plays an important role in the production of CNF from glucose. Therefore, fermentations were carried out to determine the optimal oxygen composition (0−50%). The optimal oxygen composition for CNF production was found to be 25%. For the mass production of BCNF, we used a series of 30-L-scale fermenters (KoBio Tech, KF-30, South Korea) under the same culture condition used with the 2.5-L jar fermenter.

Fibrillation and purification

After the fermentation process, the resulting broth including BCNFs was homogenised using a general homogeniser (Homogenizer HG-15A, Daehan Science, Republic of Korea). Then, the homogenised fermentation broth was passed through a microchannel (size 200 μm, Interaction chamber) of a nano disperser (ISA-NH500, Ilshin autoclave, Republic of Korea) under a pressure of 1500 bar. The well-homogenised BCNF solution was centrifuged under high pressure to obtain a cellulose precipitate. The precipitate was heated for 2 h in 0.1 N NaOH aqueous solution at 90 ºC to hydrolyse the cells and impurities existing between the BCNFs, and the resulting mixture was washed thoroughly with distilled water to obtain purified BCNFs via repeated centrifugation until the conductivity of the supernatant became less than 10 μS/cm.

Preparation of the BCNF separator

Considering the large scale roll-to-roll process of battery manufacturing, the introduction of an appropriate pore forming agent should be carefully considered, that can provide uniform pore formation and have excellent compatibility with other battery components. In order to easily produce large quantities of uniform non-woven BCNF membranes, purified BCNF was mixed with propylene carbonate (PC) serving as a foaming agent and carboxymethylcellulose (CMC) (MW ~90 kDa) could also be added to control the air permeability of the separator by interrupting hydrogen bonding between CNFs. Remarkably, most of the reported pore-forming agents induced aggregation of fibrillated CNFs or required further washing with toxic solvents. However, PC, which is known as a common electrolyte component, is well-soluble in a CNF suspension and mostly evaporates during the drying process. The pore forming mechanism is thought to be due to the difference of vapour pressure between water and PC. As the water evaporates first, the hydrogen bonds are built between CNFs in the presence of PC, and then, the pores are formed as PC evaporates, as shown in fig. S9. The BCNF slurry was prepared as follows: a solution of BCNF (0.6 g) in H_2O (120 g) was mixed with PC (2.4 g) and CMC (0.12 g) to obtain high air permeability, below 200 s/100 cm^3. Then, the resulting slurry was coated on a polyethylene terephthalate (PET) film (240 mm × 300 mm) using a micrometre applicator. The coated slurry was dried in an oven for 90 min. Subsequently, the BCNF separator was detached from the PET substrate and its tensile strength and air permeability was evaluated using an LRX-PLUS Universal Testing Machine (Lloyd instruments, UK) and Oken Type Air Permeability Tester EGO-1-55-1MR (ASAHI SEIKO CO., LTD, Japan), respectively. The porosity (31.4 %) and average pore size (53.6 nm) of as-obtained BCNF membrane were measured by mercury porosimeter (Autopore IV9500, Micromeritics) (fig. S9).

Characterization of the BCNF separator

After filtering the cultivated supernatant using a 0.22-μm syringe filter, glucose and extracellular metabolites were quantified using a HPLC instrument (Waters) equipped with an Aminex HPX-87H column (300 mm × 7.8 mm, Bio-Rad). A mobile phase of 2.5 mM H_2SO_4/0.9% (v/v) acetonitrile at a flow rate of 0.5 ml/min was used. Products were detected by refractive index measurement and a diode array detector. For the quantification of cellulose, the cellulose pads were washed with 0.1 N NaOH and rinsed several times with water and freeze-dried at −80 ºC to determine the production and yield. The thermal behaviour of the separators was analysed up to 400 °C with a heating rate of 10 °C/min using a thermomechanical analyser (TMA Q400, Waters). X-ray diffraction was carried out on a Bruker D8 Advance X-ray diffractometer under Cu $K\alpha$ radiation in the 2θ range of 10–70°. The morphology of the BCNF was observed via field-emission scanning electron microscopy (Nova NanoSEM 450, FEI), operated at 5 kV and transmission electron microscopy (Tecnai G^2, FEI), operated at 200 kV. X-ray photoelectron spectroscopy was carried out on a PHI Quantera II (ULVAC-PHI, Inc.) using Al $K\alpha$ X-ray (hv = 1486.6 eV). Fourier-transform infrared spectra were collected on a Varian 670-IR FT-IR spectrometer (Agilent Technologies Inc.) in the attenuated total reflectance mode. Raman spectra were obtained using an inVia Raman microscope (Renishaw) equipped with a 514-nm excitation laser source (~1 mW power). Differential scanning calorimetry was performed on Discovery DSC (TA instruments) in the temperature range of 25–300 °C at a heating rate of 5 °C min^{-1}. Solid-state NMR spectroscopy was performed on Bruker Avance HD-III consoles corresponding to ^1H Larmor frequency of 700.13 MHz (AVANCE HD-III, 16.4T). ^{13}C cross polarization magic angle spinning NMR experiments were performed with a spinning frequency of 15 kHz. Under the ^{13}C cross polarization condition, a cross polarization contact time of 2000 μs and delay time of 5.0 s were used. Pyrolysis-gas chromatography-mass spectroscopy was performed using a PY-

2020iD double-shot pyrolyser (Frontier Lab) connected to an Agilent 7890B series gas chromatograph (Agilent Technologies) coupled with an Agilent 5977A MSD series mass spectrometer (Agilent Technologies). An Agilent 7890A series gas chromatograph (Agilent Technologies) coupled with an Agilent 5975C MSD series mass spectrometer (Agilent Technologies) was used for the evolved gas analysis (EGA).

Electrode and electrolyte preparation for the battery

The positive electrode materials, $LiNi_{0.6}Co_{0.2}Mn_{0.2}O_2$ (NCM622) and $LiNi_{0.85}Co_{0.10}Al_{0.05}O_2$ (NCA), were purchased from Ecopro Co. LTD. (South Korea) and used as a mixture with NCM622: NCA ratio of 8:2. A slurry was prepared with the weight ratio of positive electrode material, denka black, and polyvinylidene fluoride (PVDF) of 96: 1.8: 2.2 and cast on both sides of a 12-μm Al foil, and then dried at 120 °C for 2 h in a vacuum oven. After pressing, a 129-μm-thick positive electrode tape was obtained. The loading level of the casted positive electrode was 40.7 mg/cm^2. Similarly, a negative electrode was prepared via a conventional tape-casting process. The weight ratio of graphite, styrene-butadiene rubber (SBR), and carboxymethyl cellulose (CMC) in the slurry was 97.5:1.5:1.0. The mixed slurry was coated on both sides of an 8-μm Cu foil and dried at 80 °C for 2 h in a vacuum oven. The full cell was designed with a negative/positive (N/P) ratio of 1.13. The electrolyte used in this study consisted of 1.15 M lithium hexafluorophosphate ($LiPF_6$) in ethylene carbonate/ethyl methyl carbonate/dimethyl carbonate (EC/EMC/DMC, 2:4:4 v/v/v) and 0.5% vinylene carbonate (VC).

18650 cell preparation

Mini-sized 18650 cells with 500 mAh capacity were built using a semi-automatic winder using 54-mm-wide and 150-mm-long cathodes, 58-mm wide and 190-mm long anodes, 65-mm-

wide CNF separators. The anode tab was spot-welded to the bottom of the 18650-can through the central mandrel hole and the can was grooved just above the roll to prevent the roll from sliding out of the can. After attaching the header, the cells took approximately 3.0 mL of the electrolyte. After filling, the cells were crimped. The cells were subjected to galvanostatic charge-discharge cycling (at 60 °C) using a Toyo system (Toscat-3100U). The cells were typically cycled between 2.8 and 4.3 V (versus Li/Li^+) at 1.0 C rate. 1 C corresponds to 600 mA g^{-1}. A constant voltage (CV) was applied until 0.05 C was achieved at 4.3 V and held for 10 min at both 2.8 V and 4.3 V. The DC-IR was determined after every 100 cycles at 25 °C. Before each experiment, the state of charge (SOC) was adjusted to 50% by drawing a 0.2 C charging current. After discharging for 10 s with a current of 1 A, DC-IR was calculated from the electric voltage difference.

Full-pouch cell preparation and Hot-box test

For hot-box test, 1.5 Ah full-pouch cells with a size of 4 mm × 40 mm × 70 mm were assembled. Prior to filling the electrolyte, the stacked cells were dried overnight at 80 °C in a vacuum oven to remove residual moisture. The assembled cells were charged up to 3.6 V, and then the cells were cut open to release the generated gas. After degassing, the cells were vacuum-sealed again and discharged to 3.0 V. The cells were formed by charging (CC/CV)/discharging (CC) between 4.3 and 2.8 V at the C/5 rate for 3 cycles. In the CC/CV step, CV was fixed at C/20. Finally, the formed cells were fully charged for the hot-box test. To evaluate the battery safety performance, the fully charged cells were placed in an oven connected to a battery tester. The temperature of the oven was linearly increased from room temperature to 170 °C at the rate of 5 °C min^{-1} and maintained there. At the same time, the cell voltage was monitored using the battery tester (Toyo, Toscat-3000U) during the test.

Reference

1 Saitou N & Nei M (1987) The neighbor-joining method: a new method for reconstructing phylogenetic trees. *Molecular biology and evolution* 4(4):406-425.

2 Kumar S, Stecher G, & Tamura K (2016) MEGA7: Molecular Evolutionary Genetics Analysis Version 7.0 for Bigger Datasets. *Molecular biology and evolution* 33(7):1870-1874.

3 Edgar RC (2004) MUSCLE: multiple sequence alignment with high accuracy and high throughput. *Nucleic acids research* 32(5):1792-1797.

4 Felsenstein J (1985) Confidence limits on phylogenies: an approach using the bootstrap. *Evolution* 39(4):783-791.

5 Nei M, Kumar S (2000) Molecular evolution and phylogenetics (Oxford University Press, New York),

6 Huerta-Cepas J*, et al.* (2017) Fast genome-wide functional annotation through orthology assignment by eggNOG-mapper. *Molecular biology and evolution* 34(8):2115-2122.

7 Huerta-Cepas J*, et al.* (2016) eggNOG 4.5: a hierarchical orthology framework with improved functional annotations for eukaryotic, prokaryotic and viral sequences. *Nucleic acids research* 44(D1):D286-293.

8 Chao Y, Ishida T, Sugano Y, & Shoda M (2000) Bacterial cellulose production by *Acetobacter xylinum* in a 50-L internal-loop airlift reactor. *Biotechnol*. *Bioeng*. 68(3):345-352.

9 Hwang JW, Yang YK, Hwang JK, Pyun YR, & Kim YS (1999) Effects of pH and dissolved oxygen on cellulose production by *Acetobacter xylinum* BRC5 in agitated culture. *J*. *Biosci*. *Bioeng*. 88(2):183-188.

10 Zhou L, Sun D, Hu L, Li Y, & Yang J (2007) Effect of addition of sodium alginate on bacterial cellulose production by *Acetobacter xylinum*. *J*. *Ind*. *Microbiol*. *Biotechnol*. 34:483-489.

11 Cavka A, *et al*. (2013) Production of bacterial cellulose and enzyme from waste fiber sludge. *Biotechnol*. *Bilfuels* 6:25-34.

12 Bankevich A*, et al.* (2012) SPAdes: a new genome assembly algorithm and its applications to single-cell sequencing. *Journal of computational biology : a journal of computational molecular cell biology* 19(5):455-477.

13 Chin CS*, et al.* (2013) Nonhybrid, finished microbial genome assemblies from long-read SMRT sequencing data. *Nature methods* 10(6):563-569.

14 Soto-Jimenez LM, Estrada K, & Sanchez-Flores A (2014) GARM: genome assembly, reconciliation and merging pipeline. *Current topics in medicinal chemistry* 14(3):418-424.

15 Tatusova T*, et al.* (2016) NCBI prokaryotic genome annotation pipeline. *Nucleic acids research* 44(14):6614-6624.

16 Kuo C-H, Teng H-Y, & Lee C-K (2015) Knock-out of glucose dehydrogenase gene in Gluconacetobacter xylinus for bacterial cellulose production enhancement. *Biotechnology and bioprocess engineering* 20(1):18-25.

17 Sambrook JF, Russel DW (2001) Molecular Cloning: A Laboratory Manual 3rd ed (Cold Spring Harbor, New York).